electronics

Communication

A Metalens Design for On- and Off-Center Focusing with Amorphous Silicon Hydrogenated (a-Si:H)-Based 1D Array in Visible Spectrum

Jawad Ali, Ashfaq Ahmad and Dong-you Choi *

Communication and Wave Propagation Laboratory, Department of Information and Communication Engineering, Chosun University, Gwangju 61452, Republic of Korea; ashfaquetb11@gmail.com (A.A.)
* Correspondence: dychoi@chosun.ac.kr

Abstract: The use of optical systems in medical imaging, computer electronics, large-scale industries, and space exploration is common. The performance of these devices is closely related to the compactness and fast responses of lenses that are used in these optical systems. Typical lenses suffer from several key issues, including limited efficiency, significant size, and the presence of diffraction-induced distortions that compromise their overall performance. Herein these limitations are addressed by designing and simulating an ultra-thin compact metalens also known as a flat lens using a dielectric metasurface. A 1D array of 31 nano-cylinders is placed on a glass substrate that is utilized for focusing the incident wave both on and off center in the focal plane using simulations. The nano-cylinders are comprised of amorphous silicon hydrogenated (a-Si:H), which has a varying radius in a 1D configuration. Amorphous silicon hydrogenated (a-Si:H) nano-cylinders are utilized for the manipulation of the phase of the incident beam working at a frequency of 474 THz. Three metalenses are introduced with focal lengths of 7.46 µm, 10 µm, and 12.99 µm, each having a numerical aperture (NA) of 0.7, 0.6, and 0.5, respectively. The designed single-array metalens showed a transmission efficiency of 73%. The nano-cylinders obtained a full 0–360 phase control that is beneficial in focusing the beam at the center and beyond the center. Symmetric focusing is obtained in the case of off-center focusing on both sides of the optical axis. The design and simulations of the metalens are performed using finite difference time domain (FDTD) simulation tools.

Keywords: ultra-thin metalens; dielectric metasurfaces; amorphous silicon hydrogenated; focal length; numerical aperture

Citation: Ali, J.; Ahmad, A.; Choi, D.-y. A Metalens Design for On- and Off-Center Focusing with Amorphous Silicon Hydrogenated (a-Si:H)-Based 1D Array in Visible Spectrum. *Electronics* **2023**, *12*, 2953. https://doi.org/10.3390/electronics12132953

Academic Editor: Yue Wu

Received: 31 May 2023
Revised: 1 July 2023
Accepted: 3 July 2023
Published: 5 July 2023

1. Introduction

The polarization, phase, and amplitude portray the wavefront of electromagnetic (EM) waves. Controlling these three parameters using the same device was impossible several years ago. Lenses [1], mirrors [2], and spatial phase modulators [3] have been utilized to control the phase. For the control of polarization, wave-plates [4] or polarization beam-splitters [5] are utilized, while absorptive [6] or reflective filters [7] are utilized for the amplitude control. Therefore, optical systems have become large and difficult to realize and miniaturize. Metamaterials enable the control of these properties using a single device. They are man-made nanomaterials in which the structure is engineered artificially for specific uses and can control light at the nanoscale. This control of light at the nanoscale provides a plethora of new phenomena and has numerous applications, such as flat lenses [8], invisibility cloaking [9], phase masks [10], and holography [11]. Similarly, they are also compatible with operating in terahertz (THz), the frequency range making them suitable for different applications, specifically as absorbers [12,13]. However, 3D metamaterials (bulk) exhibit losses and are not ideal for operation. Therefore, we utilize metasurfaces for the realization of different devices. Metasurfaces are 2D ultra-thin materials utilized to avoid losses in the third dimension and can be artificially engineered [14]. A dielectric metamaterial (DM) is utilized because it shows low losses in both the transverse electric (TE) and transverse magnetic (TM) modes compared to metallic materials, which exhibit high losses and require extra masking for protection [15]. DMs with a complex refractive index ($n' = n + ik$) $n > 2$ and an absorption coefficient $k \approx 0$ should be adopted to obtain high transmission and full control over the phase [16]. This is because low absorption yields high transmission, and a high refractive index provides full 0 to 2π-phase control, which allows for deflection of the beam at a certain angle [17]. The exceptional control over light manipulation, broadband performance, compact form factor, and design flexibility offered by metasurfaces make them an ideal choice for incorporating into optical instruments in the form of metalenses. The conventional lenses are generally large, expensive, and require a significant amount of time for their production [18]. They rely on phase accumulation along the passage of light propagation to focus plane waves at a specific location. Furthermore, they exhibit high transmission losses due to absorption in the visible and near-infrared (NIR) regions [19]. Accordingly, integrating these large devices with modern optical technologies presents a significant challenge, and to fill this gap, researchers have diverted their attention to metamaterials, especially metasurface-based metalenses [20]. The design of high-efficiency achromatic metalenses that have a large operation bandwidth using bilayer architecture is presented in [21]. A multi-foci metalens is also presented as capable of both spectrum and polarization recognition and reconstruction in just a single shot [22]. Similarly, a silicon-based THz metalens is constructed using dynamic phase to obtain single-handed circular polarization conversion [23]. The design of efficient metalenses has experienced a long struggle owing to material losses and the non-compatibility of the structure. Metalenses rely on the manipulation of light at subwavelength scales, which can lead to significant optical losses [24]. Metalenses often involve intricate and complex structures, which may not be compatible with traditional fabrication techniques or materials [25]. Several designs have been presented for the construction of plasmonic metasurfaces [26], high-contrast transmit arrays [27], and gratings [28]; however, their functionalities are limited. In the designs proposed so far, plasmonic metalenses have demonstrated low efficiency related to their ohmic losses [29], and transmitted array operations that demonstrate high transmission efficiency [30]. The operations of these metalenses are restricted to the near-infrared (NIR) regions, and because of their constituent materials, they demonstrate optical losses in the visible region. In 2016, Capasso et al. first reported metalenses in the visible band with an amorphous titanium oxide metasurface using bottom-up nanofabrication via atomic layer deposition (ALD) [31]. A design of high-efficiency achromatic metalenses that have a large operation bandwidth using bilayer architecture is presented [21]. A multi-foci metalens is also presented that is capable of both spectrum and polarization ellipticity recognition and reconstruction in just a single shot [22]. Titanium dioxide (TiO_2) and gallium nitride (GaN) have demonstrated promising results with a high refractive index (n) and low extinction coefficient (k); however, they have a high aspect ratio and require complex and costly fabrication techniques for realization [32]. On the other hand, the refractive index of TiO_2 is high, which can cause chromatic aberration in metalenses designed for the visible region. This can be a problem if the metalens is intended to operate over a broad wavelength range. Khorasaninejad et al. [31] note that chromatic aberration can limit the bandwidth of metalenses designed with TiO_2 in the visible region. TiO_2 exhibits high absorption at certain wavelengths in the visible region, which limit the efficiency of the designed metalens with this material. When considering the operation of metalenses, it is important to have materials that exhibit minimal absorption of visible wavelengths. TiO_2 nano-cylinders, however, tend to absorb visible light, which is beneficial in solar cell applications [33] but is not suitable for the designing of metalenses. This absorption can significantly affect the performance of metalenses, as it leads to a loss of energy and reduces the efficiency of focusing or manipulating light. As a result, TiO_2 nano-cylinders are considered less suitable for metalens applications where high transmission and low absorption of visible wavelengths are desired for optimal performance. Similarly, in recent studies, the metalens design has been somewhat refined in the form of super-oscillatory focusing [34], widefield imaging [35], and reflective metalenses [36]. Additionally, there has been extensive research on other 2D layered materials, such as graphene and transition metal dichalcogenides (TMDCs) represented by the formula MX_2, where M denotes a transition metal atom (such as Mo or W) and X represents a chalcogen atom (such as S, Se, or Te). These materials have garnered significant attention as promising candidates for future nanometric optoelectronic devices. Their strong light–matter interactions, attributed to the effects of 2D quantum confinement, make them particularly attractive for a wide range of applications in the field of optics and photonics. [37,38]. Flat lenses employing 200 nm thick graphene oxide (GO) films have demonstrated remarkable capabilities in achieving efficient three-dimensional (3D) focusing with high resolution (32%) [39]. This is attributed to the notable refractive index and absorption modulation achievable through the laser reduction of GO. However, it should be noted that reducing the thickness of GO beyond this point may result in a compromise in focusing efficiency and resolution. While optical lenses utilizing multi-layer graphene [40] and transition metal dichalcogenides (TMDCs), such as MoS_2 [41], have been successfully demonstrated, they face limitations in terms of focusing resolution ($>10\lambda$) and efficiency (<1%) due to the constrained phase and amplitude modulation achievable with current technologies. While the existing designs of metalenses have provided insights into their characteristics, they have exhibited certain limitations regarding miniaturization, aberration correction, and the incorporation of multiple focal lengths within a single design. Notably, the majority of simulated designs have emphasized on-center focusing, while off-center focusing capabilities have remained relatively unexplored. Additionally, most of the designs presented so far are 2D arrays that have limitations in terms of their fabrication, compactness, and efficiency [1]. To address these gaps, we present a novel proposal for a compact 1D array comprising 31 unit cells that exhibits multiple focusing functionalities in the visible region while minimizing aberration and ensuring notable efficiency. This single design offers versatile applications, enabling both on-center and off-center focusing with varying focal lengths and numerical apertures (NA) within the visible range. The phase required at each position can be determined according to the phase distribution formula [42]. Phase manipulation of the incident light can be performed using both the geometric phase mechanism and Hugen's principle techniques [43]. The phase of the incident waves is changed by the geometry as well as the manipulation of incident light at the wavefront in nano-cylinders at the aperture. These nano-cylinders act as phase shifters that can be considered as reduced waveguides whose effective refractive index n_{eff} is responsible for the phase change of the incident wave. A phase delay is produced in most cases due to these nano-cylinders that are responsible for the beam steering by changing n_{eff}. Similarly by customizing the position and lateral size of the nano-cylinders [44], the n_{eff} can be tailored. The cross-section of the structure can be tailored to produce either a polarization-dependent [45] or -independent [46] optical response from the scatterers. Titanium dioxide (TiO_2), gallium nitride (GaN), graphene, and transition metal dichalcogenides (TMDCs) 2D layers are mostly considered, but they have discrepancies in the form of high chromatic aberration, elevated absorption, and large sizes, which make them less efficient. Here we present an amorphous silicon hydrogenated (a-Si:H) nano-cylinders-based 1D structure that is more compact as well as showing reduced chromatic aberration and absorption in the visible range. The proposed structure exhibits full-phase control 0–360° of the incident beam with high transmission efficiency.

The remainder of this paper is structured as follows: The methodology, which is comprised of the unit cell and array designing with their respective parameters, is discussed in Section 2. The simulated results for single-spot focusing are presented in Section 3. Finally, Section 4 concludes the study by summarizing the findings, discussing their implications, and suggesting future research directions.

2. Methodology

The designed unit cells can operate as phase shifters, enabling them to manipulate the incident light. Phase shifters offer complete phase control of the incoming light wave, ranging from 0–360°, allowing it to be precisely steered and focused onto a single point. The phase of the incoming light is altered as it passes through the unit cells with specified radii by the focal length. Phase shifters can modify the light at the wavefront of incoming waves, making them more adaptable for practical applications. By altering the radius of the nano-cylinders, it is possible to modify the phase and amplitude of the transmitted wave. The phase profile imparted by each nano-cylinder at the position (x, y) for focusing is given by,

$$\phi(x,y) = 2n\pi - \frac{2\pi}{\lambda}\left(\sqrt{x^2+y^2+f^2} - |f|\right) \tag{1}$$

where x and y are the unit cell coordinates on the metasurface, f is the focal length, and λ is the working wavelength in free space. The design for a metalens, which possesses the ability to focus the incident wave on- and off-centers, is created using nano-cylinders comprised of amorphous silicon hydrogenated (a-Si:H). To determine the phase of each scatterer, a lensing function based on the x-coordinate of the unit cell is used. The incident wave is effectively focused at the center utilizing nano-cylinders, employing a phase manipulation mechanism to attain precise and comprehensive control over the phase of the incident wave. The position along with the n_{eff} of the a-Si:H nano-cylinders are also responsible for the phase change that focuses the incoming beam at the center. The phase profile of the incoming wave is defined by the following expressions for single spot on-center focusing:

$$\phi(x) = 2\pi - \frac{2\pi}{\lambda}\left(\sqrt{x^2+f^2} - |f|\right) \tag{2}$$

The value of f represents the focal length, π corresponds to the operating wavelength, and x denotes the position of the unit cell on the substrate. Equation (2) provides the phase distribution over the metalens aperture as a function of the x-coordinate and focal length. To achieve the desired focus point in the xz-plane, each nano-cylinder must be placed at a specific position along the substrate. To achieve off-center focusing, the position of each unit cell must be changed, which in turn produces a phase delay. By controlling the size and spacing of the nanostructures, you can control the phase delay and, consequently, the focusing. The phase delay introduced by each nanostructure determines the overall phase profile of the metalens as it is proportional to the distance the light travels between two unit cells. The distance between the unit cells is determined by the position of the unit cells in the metasurface. By changing the position of the unit cells in the metasurface, a metalens with a varying phase profile is created. This varying phase profile can be used to focus incident waves at a point off the optical axis. The phase profile of the nano-cylinders for off-center focusing is obtained using the following equation:

$$\phi(x) = 2\pi - \frac{2\pi}{\lambda}\left(\sqrt{(x^2-x_1^2)+f^2} - |f_a|\right) \tag{3}$$

where

$$f_a = \sqrt{x_1^2+f^2} \tag{4}$$

$$x_1 = \pm 5 * P \tag{5}$$

The incident light is focused at an arbitrary position by changing the position of the unit cell in the focal plane (xz-plane). The position x of the unit cell will be changed by a factor x_1 that is equal to ± 5 times the periodicity of the unit cell along the x coordinate, as denoted by Equation (5). Arbitrary focal length (f_a), which shows the focal length of the point off the optical axis, is also one of the factors for off-center focusing and is achieved by adding x_1 and focal length f, as denoted in Equation (4). The assigned value is positive for right-side focusing and negative for left-side focusing along the x coordinate. By utilizing identical parameters, including the NA and focal length, two separate outcomes were achieved for off-center focusing on both positive and negative sides.

For both on-center and off-center focusing simulations, we employed a consistent simulation environment using Lumerical FDTD (finite difference time domain) method. In our simulations, a plane wave source was illuminated along the z-axis, with a specific frequency of 474 THz corresponding to the desired wavelength of interest. This choice of source configuration allows for controlled and reproducible excitation of the metasurface structure. To characterize the performance of the designed metalens, we utilized a Discrete Fourier Transform (DFT) monitor. This monitor was strategically placed to capture the response of the transmitted waves and precisely determine the location of the focal point. By measuring the focal location, we were able to evaluate the focusing capability of the metalens structure. In addition to the focal point analysis, we performed a cross-sectional analysis to assess the efficiency of the metalens in terms of transmission and absorption. This analysis provided valuable insights into the performance and overall effectiveness of the designed metalens. To ensure accurate and reliable simulation results, appropriate boundary conditions were implemented along the x-, y-, and z-axes. These boundary conditions helped create a suitable computational domain for capturing the behavior of the electromagnetic waves and interactions with the metasurface structure. A single design was used in the same simulated environment.

2.1. Unit Cell Design

The material utilized to design the unit cell in this study is amorphous silicon hydrogenated (a-Si:H), which has a comparatively high refractive index (n = 3.247) with minor losses due to a low extinction coefficient (k = 0.0471). A higher refractive index results in a decreased aspect ratio [47]. The maximum aspect ratio (AR) sets a bound on the minimum radius (R) of a nano-cylinder that can be readily handled in fabrication, expressed as:

$$AR = \frac{H}{2R_{\text{min}}}$$

The height of the nano-cylinder is denoted by H, while the minimum radius is represented as $2R_{\text{min}}$. It should be noted that the maximum radius of the cylinder must not exceed the size of the unit cell. Nano-cylinders with a lower aspect ratio (AR) are preferred over those with a higher aspect ratio due to their increased durability and the avoidance of the need for extra metal masks during fabrication [48]. This paper discusses an aspect ratio (AR) of 5 for the nano-cylinders with the smallest radius of 40 nm and a height of 400 nm, which is significantly smaller compared to that of TiO_2 and GaN, which are 7.5 [49] and 12 [32], respectively. Plasma-enhanced chemical vapor deposition (PECVD) enables the low-temperature deposition of hydrogenated amorphous silicon (a-Si:H) [50]. Compared to standard amorphous silicon (a-Si), a-Si:H exhibits reduced absorption at visible frequencies due to the presence of hydrogen impurities, which effectively decrease the defect density of the material [51,52]. Furthermore, a-Si:H with a high refractive index offers strong confinement of wave into the nano-cylinder, which results in full hold over the phase of refracting wave. The a-Si:H nano-cylinder introduces phase retardation to the refracted wave, which can be tuned over 0–360° by varying the radius of a-Si:H nano-cylinder.

To optimize the unit cell, we performed a parameter sweep on the radius using finite difference time domain (FDTD) simulations. By varying the radius within a specific range, we evaluated the transmission efficiency and phase change at each point in accordance with the change in the radius of the unit cell. Throughout the optimization process, the height and periodicity of the unit cells were kept constant. The transmission and phase profiles of the proposed unit cell obtained from the parameter sweep on radius are illustrated in Figure 1a, which provides details about the transmission and phase response of the unit cell with varying radii. The transmission and phase profiles of the proposed unit cell demonstrate the effectiveness of the design. The average transmission efficiency is 73% at 633 nm, which is achieved due to the low absorption characteristics of the designed a-Si:H nano-cylinders. To design the unit cell, the essential parameters such as the radius, height, and periodicity of the unit cell are inserted into a finite difference time domain (FDTD) simulation software tool (Lumerical FDTD). Phase control (0–360°) made it possible to focus the incident beam on- and off-center using nano-cylinders. It is observed that for the range of R from 40 nm to 140 nm with periodicity P = 300 nm and H = 400 nm, the maximum transmission amplitude along with full phase control is achieved. The unit cell is positioned on a glass substrate composed of SiO_2, with a subwavelength size. The phase and transmission profiles of the unit cell are due to the relatively high refractive index ($n > 2$) and low absorption ($k \approx 0$) of the a-Si:H nano-cylinders. The refractive index (n) corresponds to the ability of the material to bend light, while the extinction coefficient (k) indicates the level of absorption. A high refractive index facilitates efficient light bending and focusing, while a low extinction coefficient implies minimal absorption of light, leading to reduced energy losses. The refractive index (n) and extinction coefficient (k) of a-Si:H over the whole visible spectrum are presented in Figure 1b [51].

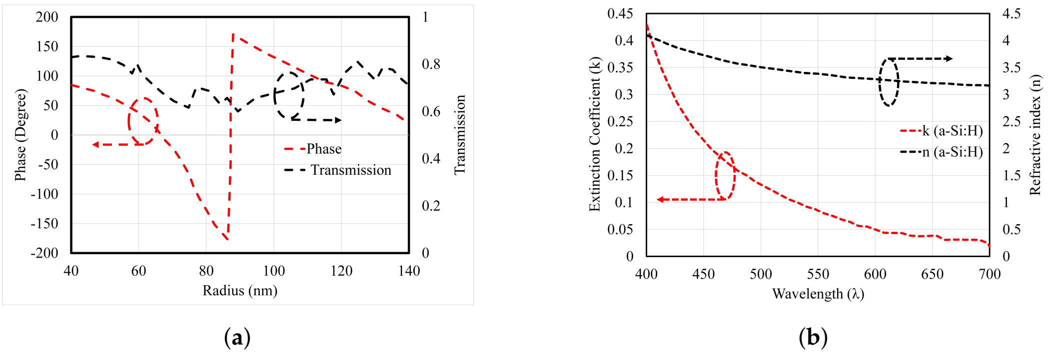

Figure 1. (**a**) Transmission and phase profile of the proposed unit cell with varying radius (**b**) The refractive index (n) and extinction coefficient (k) of a-Si:H for the entire visible spectrum [51].

Schematics of the proposed unit cell with boundary conditions along the coordinates are illustrated in Figure 2a. The x- and z-axes were bounded by perfectly matched layer (PML) boundary conditions, whereas periodic boundary conditions were employed along the y-axis. Figure 2b illustrates the side view of the metalens unit, where H is the height of the a-Si:H nano-cylinder that has a value of 400 nm. The top view of the unit cell is illustrated in Figure 2c, which indicates the radius (R).

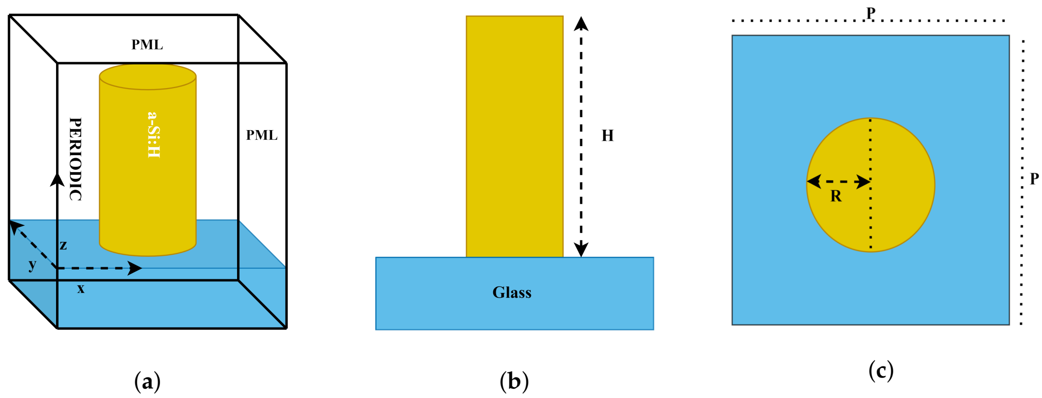

Figure 2. (**a**) Schematics of the unit cell: a-Si:H nano-cylinder on a glass substrate. (**b**) Side-view of the unit cell showing the height H. (**c**) Top-view of the unit cell portraying radius R, and periodicity P of the a-Si:H nano-cylinders.

2.2. Proposed Array

A 1D array of 31 unit cells was placed on a glass substrate to engineer the phase of the incident wave by adjusting the position of the unit cells in the xz-plane as illustrated in Figure 3. The x span of the substrate is 9 µm, y span is 0.3 µm, and z span is 2.2 µm, while the total length of the structure is 5.58 µm. The dimensions of the substrate are compatible with the arrangement of the unit cells and are enough to accommodate them to design an efficient array. Similarly, the a-Si:H nano-cylinders are placed in a varying radius manner in which the radius is larger at the center and shows an exponential decrease when moving toward the edges on both sides. The purpose of this arrangement is to accommodate the phase of the incident wave by creating a phase delay using the nano-cylinders. The optical device presented is a polarization-insensitive metalens that is utilized to focus the incident wave on- and off-center. These metalenses, which are based on a-Si:H, exhibited high efficiencies compared with conventional designs based on TiO_2 and GaN. Circular geometry was considered because of its polarization-insensitive behavior [17].

The principle of the arrangement of the array is based on two things: one is the propagation phase mechanism, which is responsible for a spatially varying phase response achieved by varying the radii of the nano-cylinders. This allows full control over the phase of the incident wave by introducing phase delay. Secondly, the position of the unit cells in the array along the substrate also plays a vital role in focusing and defining the direction of the transmitted wave. The properties of on-center and off-center focusing are incorporated in the unit cells using these techniques along with the propagation phase mechanism. Both mentioned properties define the working principle of the arrangement of the unit cell.

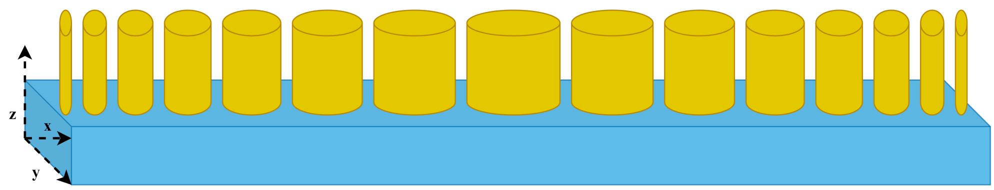

Figure 3. Schematics of the metalens in the xz-plane when an array of a-Si:H nano-cylinders is placed on a glass substrate.

3. Results and Discussion

A single metalens design was developed to achieve focused incident waves at specific wavelengths. The metalens demonstrates its focusing capabilities at three distinct focal lengths that are 7.46 µm, 10 µm, and 12.99 µm. These focal lengths were carefully selected to correspond to the desired numerical aperture (NA) values of 0.7, 0.6, and 0.5, respectively. By incorporating multiple focal lengths, a comprehensive evaluation of the metalens' performance across different numerical apertures is achieved. The selection of these specific focal lengths allows for a thorough investigation of the metalens' focusing abilities within the visible region. Through adjustments made within the FDTD Lumerical software, the values of the focal lengths are modified for each simulation manually, enabling a detailed analysis of the metalens' design under varying conditions. This approach provides valuable insights into the metalens' behavior and performance in achieving precise on- and off-center focusing in the xz-plane. The results for both on- and off-center focusing are presented in this section that portrays the multi-functionality of the 1D metalens that can be used for different focal lengths. This study presents a comprehensive analysis of the metalens' performance in achieving on-center focusing, as demonstrated in Figures 4a–c and 5. The electric-field intensity distribution within the focal region (xz-plane) provides valuable insights into the metalens' focusing capabilities. The electric-field intensity distribution reveals the precise focus achieved at the center, resulting in a well-defined focal spot that emulates the behavior of a conventional curved lens. This characteristic highlights the effectiveness of the metalens in directing incident waves to a specific focal point with accuracy. To further illustrate the sharpness of the focal spot, Figure 5 displays the intensities of the focused waves in the horizontal plane at 633 nm for the given focal lengths. The intensity distribution in Figure 5 serves as additional evidence, corroborating the metalens' ability to focus on-center on incoming plane waves.

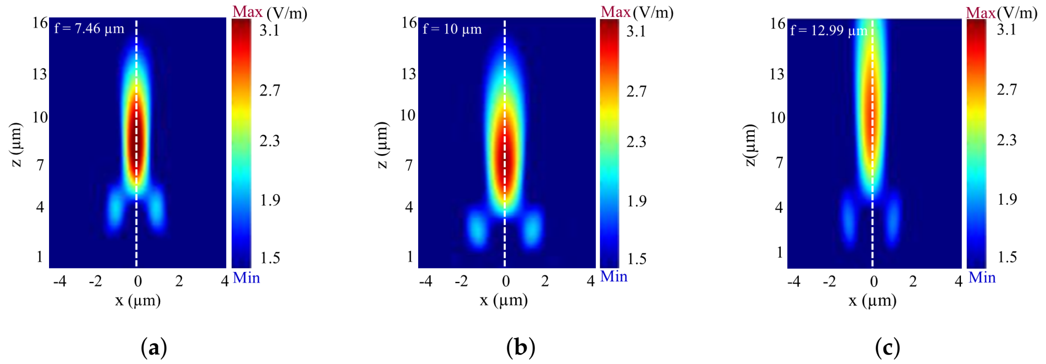

Figure 4. (**a**–**c**) Electric field intensity distribution of the incoming wave for on-center focusing for focal lengths 7.46 µm, 10 µm, and 12.99 µm.

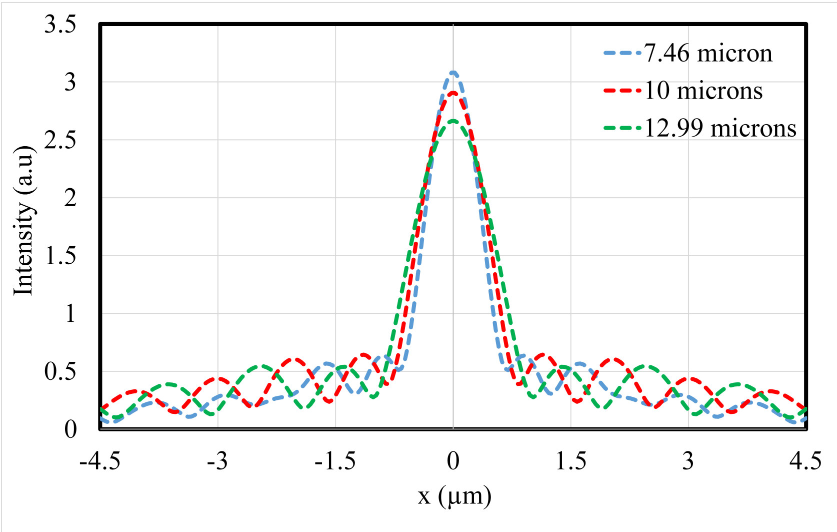

Figure 5. Intensities of the transmitted energies indicated at $x = 0$ for focal lengths 7.46 µm, 10 µm, and 12.99 µm.

In addition to achieve on-center focusing, the designed metalens also exhibited the ability to focus incident beams at off-center points by manipulating the phase of the incident beam. This off-center focusing capability is achieved by adjusting the position of the unit cell along the glass substrate and implementing a phase delay operation by the unit cell. The electric field intensity distribution and focal spot intensity of the metalens, with a focal length of 7.46 µm and a numerical aperture (NA) of 0.7, was investigated for off-center focusing. Figure 6a,b visually depict the off-center focusing capabilities of the metalens, showcasing the concentration of energy in the xz-plane away from the optical axis. Furthermore, Figure 7 provides a comprehensive illustration of the metalens' performance in off-center focusing by displaying the intensities on both the positive and negative sides. This visualization highlights the metalens' ability to focus incident waves proportionally on both sides, indicating its symmetrical response during off-center focusing. The symmetric behavior exhibited by the metalens ensures a balanced and precise concentration of energy at the desired off-axis focal points.

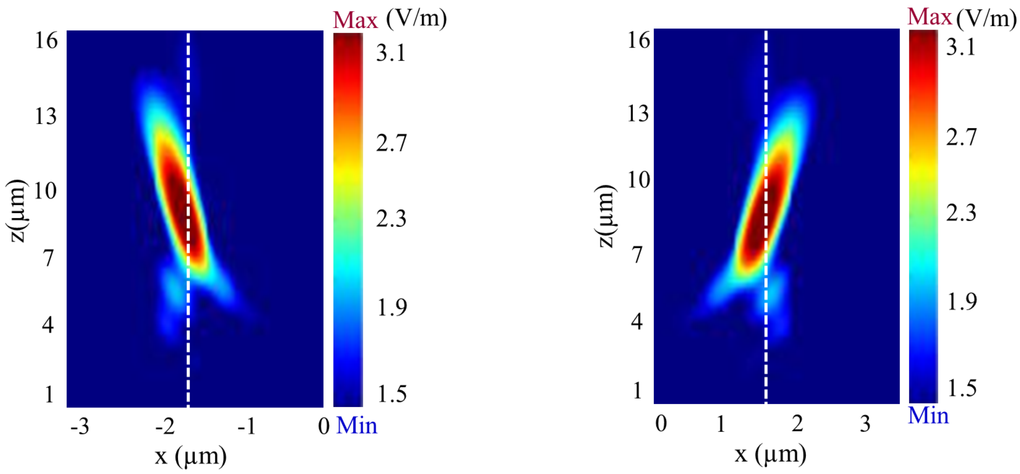

Figure 6. (**a**,**b**) Electric the field intensity distribution of the incoming wave along the positive and negative side for off-center focusing using focal length 7.46 µm in the xz-plane.

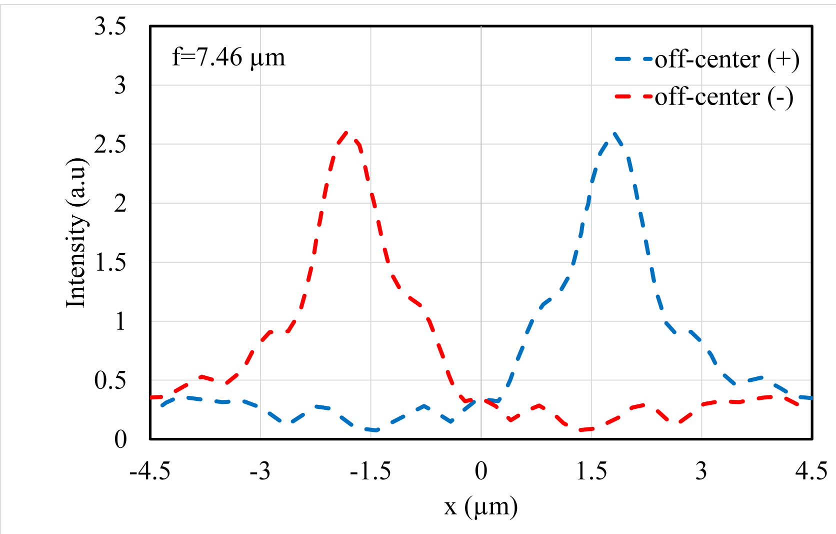

Figure 7. Intensities of the transmitted energies shown at $x = -1.78$ µm, 1.78 µm.

A similar methodology was utilized to achieve off-center focusing in the xz-plane using the same designed metalens by changing the focal length to 10 µm and numerical aperture (NA) to 0.6, as depicted in Figure 8a,b. These figures display the electric field intensity distribution of the focal spot at arbitrary points in the xz-plane, providing a visual representation of the metalens' off-center focusing capabilities. Figure 9 enhances the analysis by presenting the intensities of the transmitted energies along the x-coordinate. This depiction showcases the balanced alignment of intensities on both sides, illustrating the symmetrical nature of the metalens' focusing behavior. The figure serves as evidence of the metalens' ability to effectively focus the incoming light off-axis, demonstrating its versatility and precision in achieving off-center focal points.

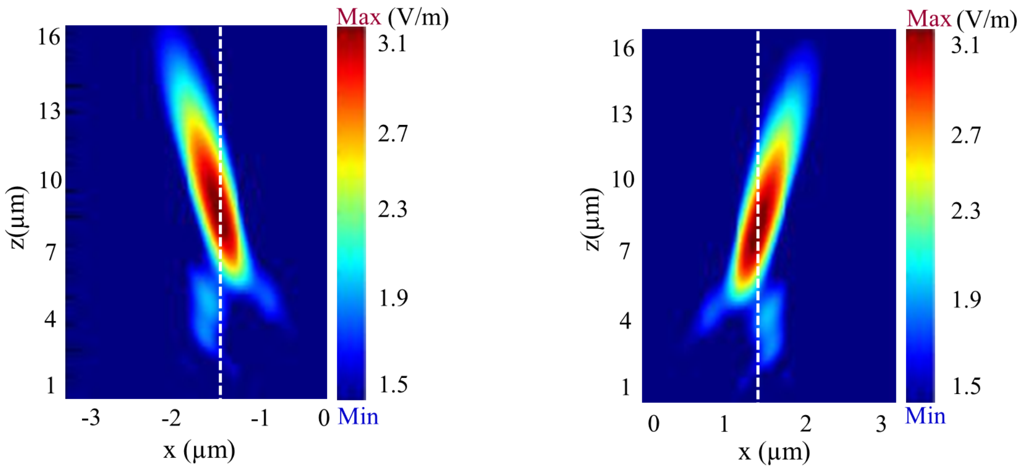

(**a**) (**b**)

Figure 8. (**a**,**b**) Electric the field intensity distribution of the incoming wave along the positive and negative side for off-center focusing using focal length 10 μm in the xz-plane.

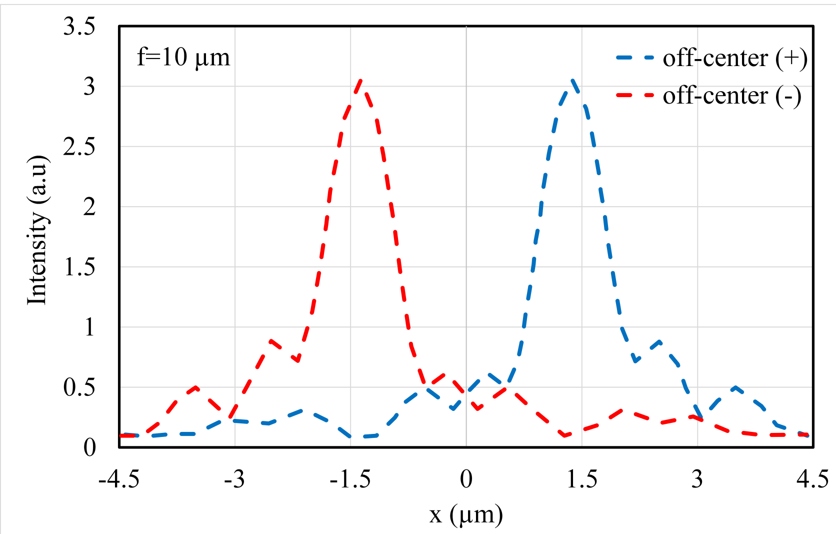

Figure 9. Intensities of the transmitted energies displayed at $x = -1.38$ μm, 1.38 μm.

The optical response of the flat lens with a focal length of 12.99 μm and a numerical aperture (NA) of 0.5 in the xz-plane is presented in Figure 10a,b. These figures showcase the electric field intensity distribution, highlighting the off-center focusing capabilities of the designed metalens. Additionally, Figure 11 displays the intensities of the transmitted energies at arbitrary points along the x-coordinate, revealing symmetrical intensities on both sides. These findings are consistent with the observations presented in Figure 10a,b.

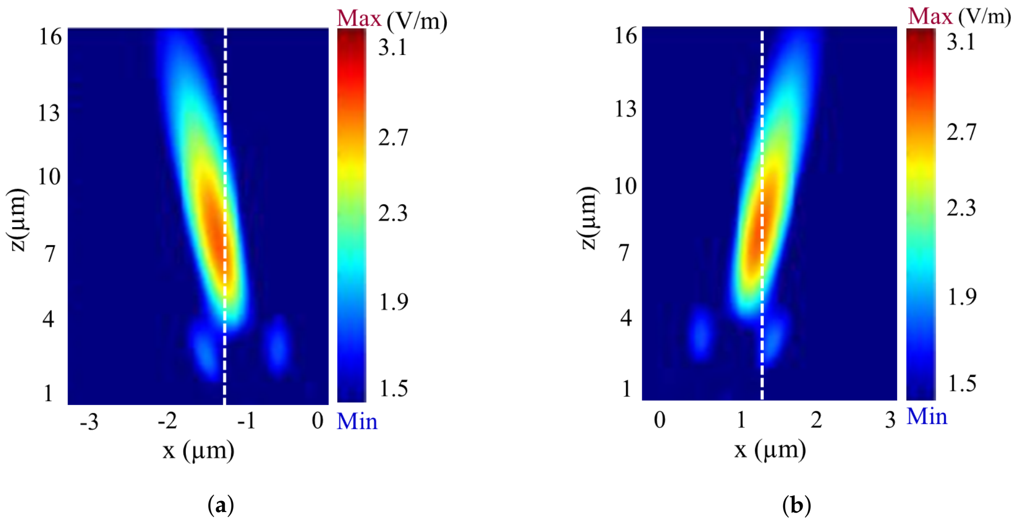

Figure 10. (**a**,**b**) Electric the field intensity distribution of the incoming wave along the positive and negative side for off-center focusing using focal length 12.99 μm in the xz-plane.

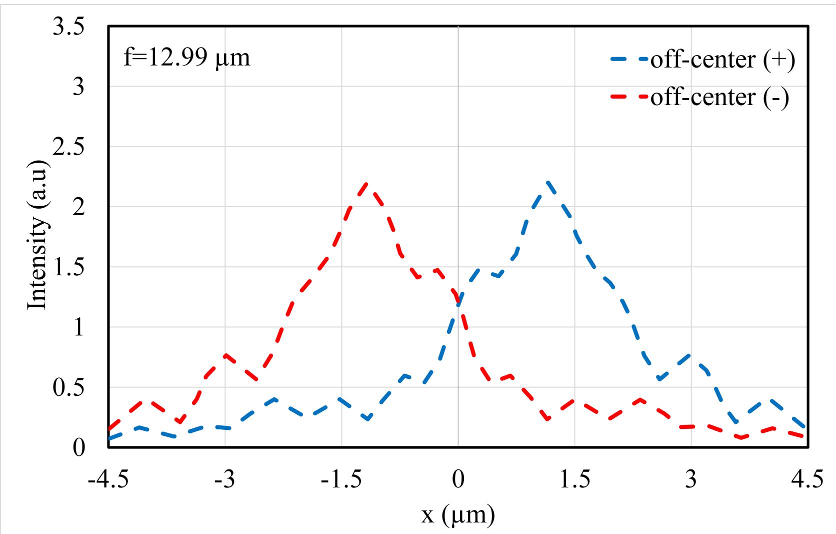

Figure 11. Intensities of the transmitted energies displayed at $x = -1.18$ μm, 1.18 μm.

Overall, these figures illustrate the effectiveness and versatility of the designed 1D metalenses as promising candidates for both on- and off-center focusing in the visible region. Owing to their ability to achieve high levels of accuracy and precision, metalenses offer exciting opportunities for numerous applications ranging from microscopy and imaging to sensing and optical communication.

4. Conclusions

The metalens proposed in this study offered a way to tailor incoming waves with their compact size and simple arrangement and resulted in unique characteristics that were achieved by manipulating the phase of the incident waves. The proposed metalens showcase a high transmission with accurate focusing at the desired focal lengths using a single design. The 1D array of unit cells is capable of both on- and off-center focusing along the optical axis, which shows the multiple functionality. The full phase control (0 to 2π) gave it the ability to bend the incoming plane wave in the direction we wanted to focus it by altering the phase of the incoming wave. The nano-cylinders were responsible for the phase delay that steers the incoming plane waves. Our design displayed versatility in its ability to focus the incident plane wave on and off the optical axis. The techniques are based on the propagation phase mechanism and the varying relative position of the unit cells. The designed metalens exhibits multiple functionalities that are portrayed by a single design with different focal lengths and NA in the visible region. The results obtained from simulations are in agreement and portray that the designed structure shows optimal efficiency with low losses as well as the ability to steer the incident waves to obtain focusing at the given focal lengths. The proposed design can be used to fabricate a flat lens that can change the phase of incoming waves and focus it on and off the optical axis. The mentioned technique can be implemented across various optical devices in approximately all optical systems, with the aim of achieving high efficiency and phase control. It possesses the ability to focus multiple times using a single design in the visible region with a high transmission efficiency that can be used for better resolution and reduced aberration. The single working wavelength and the material's refractive index also reduce the aberration errors that are found in conventional optical systems. In the future, this design can be extended to operate at different wavelengths in the visible spectrum and also beyond it. Similarly, this design can be used to focus the incident wave on a dual spot both on and off center.

Author Contributions: Conceptualization, J.A. and A.A.; data curation, J.A. and A.A.; funding acquisition, D.-y.C.; methodology, J.A. and A.A.; project administration, A.A. and D.-y.C.; resources, A.A. and J.A.; software, J.A. and A.A.; supervision, D.-y.C.; validation, A.A. and D.-y.C.; writing—original draft, J.A.; writing—review and editing, A.A. All authors have read and agreed to the published version of the manuscript.

Funding: This study was supported by a research fund from Chosun University (2022).

Data Availability Statement: The data can be provided upon request from the authors.

Conflicts of Interest: The authors declare no conflict of interest.

References

1. Chen, M.K.; Wu, Y.; Feng, L.; Fan, Q.; Lu, M.; Xu, T.; Tsai, D.P. Principles, functions, and applications of optical meta-lens. *Adv. Opt. Mater.* **2021**, *9*, 2001414. [CrossRef]
2. Cui, J.; Huang, C.; Pan, W.; Pu, M.; Guo, Y.; Luo, X. Dynamical manipulation of electromagnetic polarization using anisotropic meta-mirror. *Sci. Rep.* **2016**, *6*, 30771. [CrossRef]
3. Fernández, E.J.; Prieto, P.M.; Artal, P. Wave-aberration control with a liquid crystal on silicon (LCOS) spatial phase modulator. *Opt. Express* **2009**, *17*, 11013–11025. [CrossRef]
4. Lammers, K.; Ehrhardt, M.; Malendevych, T.; Xu, X.; Vetter, C.; Alberucci, A.; Szameit, A.; Nolte, S. Embedded nanograting-based waveplates for polarization control in integrated photonic circuits. *Opt. Mater. Express* **2019**, *9*, 2560–2572. [CrossRef]
5. Lee, W.S.; Nirantar, S.; Headland, D.; Bhaskaran, M.; Sriram, S.; Fumeaux, C.; Withayachumnankul, W. Broadband terahertz circular-polarization beam splitter. *Adv. Opt. Mater.* **2018**, *6*, 1700852. [CrossRef]
6. Li, Z.; Butun, S.; Aydin, K. Ultranarrow band absorbers based on surface lattice resonances in nanostructured metal surfaces. *ACS Nano* **2014**, *8*, 8242–8248. [CrossRef] [PubMed]
7. Iazikov, D.; Greiner, C.; Mossberg, T. Apodizable integrated filters for coarse WDM and FTTH-type applications. *J. Light. Technol.* **2004**, *22*, 1402–1407. [CrossRef]
8. Wang, H.; Yang, Y. Optics Frontiers Online 2020: Micro and Nanophotonics (OFO-4 2020). In *Optics Frontiers Online 2020: Micro and Nanophotonics (OFO-4 2020)*; SPIE: Bellingham, WA, USA, 2020; p. 11608.
9. Zouros, G.P.; Kolezas, G.D.; Almpanis, E.; Tsakmakidis, K.L. Three-Dimensional Invisibility to Superscattering Induced by Zeeman-Split Modes. *arXiv* **2020**, arXiv:2008.00121.
10. Ren, H.; Fang, X.; Jang, J.; Bürger, J.; Rho, J.; Maier, S.A. Complex-amplitude metasurface-based orbital angular momentum holography in momentum space. *Nat. Nanotechnol.* **2020**, *15*, 948–955. [CrossRef]
11. Wang, Q.; Xu, Q.; Zhang, X.; Tian, C.; Xu, Y.; Gu, J.; Tian, Z.; Ouyang, C.; Zhang, X.; Han, J.; et al. All-dielectric meta-holograms with holographic images transforming longitudinally. *ACS Photonics* **2018**, *5*, 599–606. [CrossRef]
12. Xiong, H.; Ma, X.; Zhang, H. Wave-thermal effect of a temperature-tunable terahertz absorber. *Opt. Express* **2021**, *29*, 38557–38566. [CrossRef] [PubMed]
13. Suo, M.; Xiong, H.; Li, X.K.; Liu, Q.F.; Zhang, H.Q. A flexible transparent absorber bandwidth expansion design based on characteristic modes. *Results Phys.* **2023**, *46*, 106265. [CrossRef]
14. Ding, F.; Pors, A.; Bozhevolnyi, S.I. Gradient metasurfaces: A review of fundamentals and applications. *Rep. Prog. Phys.* **2017**, *81*, 026401. [CrossRef] [PubMed]
15. Lin, B.q.; Lv, L.t.; Guo, J.; Wang, Z.; Huang, S.; Huang, B. Ultra-wideband anomalous reflection realised by a gradient metasurface. *IET Microwaves Antennas Propag.* **2020**, *14*, 1424–1430. [CrossRef]

16. Zhang, Q.; Li, M.; Liao, T.; Cui, X. Design of beam deflector, splitters, wave plates and metalens using photonic elements with dielectric metasurface. *Opt. Commun.* **2018**, *411*, 93–100. [CrossRef]
17. Ahmed, H.; Ali, M.M.; Ullah, A.; Rahim, A.A.; Maab, H.; Khan, M. An ultra-thin beam splitter design using a-Si: H based on phase gradient metasurfaces. *J. Nanoelectron. Optoelectron.* **2019**, *14*, 1339–1343. [CrossRef]
18. Engelberg, J.; Levy, U. The advantages of metalenses over diffractive lenses. *Nat. Commun.* **2020**, *11*, 1991. [CrossRef]
19. Groever, B.; Chen, W.T.; Capasso, F. Meta-lens doublet in the visible region. *Nano Lett.* **2017**, *17*, 4902–4907. [CrossRef]
20. Zheng, Y.; Xu, M.; Pu, M.; Zhang, F.; Sang, D.; Guo, Y.; Li, X.; Ma, X.; Luo, X. Designing high-efficiency extended depth-of-focus metalens via topology-shape optimization. *Nanophotonics* **2022**, *11*, 2967–2975. [CrossRef]
21. Wang, Y.; Fan, Q.; Xu, T. Design of high efficiency achromatic metalens with large operation bandwidth using bilayer architecture. *Opto-Electron. Adv.* **2021**, *4*, 200008. [CrossRef]
22. Gao, H.; Fan, X.; Wang, Y.; Liu, Y.; Wang, X.; Xu, K.; Deng, L.; Zeng, C.; Li, T.; Xia, J.; et al. Multi-foci metalens for spectra and polarization ellipticity recognition and reconstruction. *Opto-Electron. Sci.* **2023**, *2*, 220026-1. [CrossRef]
23. Li, J.; Wang, G.; Yue, Z.; Liu, J.; Li, J.; Zheng, C.; Zhang, Y.; Zhang, Y.; Yao, J. Dynamic phase assembled terahertz metalens for reversible conversion between linear polarization and arbitrary circular polarization. *Opto-Electron. Adv.* **2022**, *5*, 210062-1. [CrossRef]
24. Boriskina, S.V.; Cooper, T.A.; Zeng, L.; Ni, G.; Tong, J.K.; Tsurimaki, Y.; Huang, Y.; Meroueh, L.; Mahan, G.; Chen, G. Losses in plasmonics: From mitigating energy dissipation to embracing loss-enabled functionalities. *Adv. Opt. Photonics* **2017**, *9*, 775–827. [CrossRef]
25. Lalanne, P.; Chavel, P. Metalenses at visible wavelengths: Past, present, perspectives. *Laser Photonics Rev.* **2017**, *11*, 1600295. [CrossRef]
26. Verslegers, L.; Catrysse, P.B.; Yu, Z.; White, J.S.; Barnard, E.S.; Brongersma, M.L.; Fan, S. Planar lenses based on nanoscale slit arrays in a metallic film. *Nano Lett.* **2009**, *9*, 235–238. [CrossRef]
27. Arbabi, A.; Horie, Y.; Ball, A.J.; Bagheri, M.; Faraon, A. Subwavelength-thick lenses with high numerical apertures and large efficiency based on high-contrast transmitarrays. *Nat. Commun.* **2015**, *6*, 7069. [CrossRef] [PubMed]
28. Khorasaninejad, M.; Aieta, F.; Kanhaiya, P.; Kats, M.A.; Genevet, P.; Rousso, D.; Capasso, F. Achromatic metasurface lens at telecommunication wavelengths. *Nano Lett.* **2015**, *15*, 5358–5362. [CrossRef]
29. Kanwal, S.; Wen, J.; Yu, B.; Chen, X.; Kumar, D.; Kang, Y.; Bai, C.; Ubaid, S.; Zhang, D. Polarization insensitive, broadband, near diffraction-limited metalens in ultraviolet region. *Nanomaterials* **2020**, *10*, 1439. [CrossRef]
30. Zhang, X.; Yang, F.; Xu, S.; Aziz, A.; Li, M. Dual-layer transmitarray antenna with high transmission efficiency. *IEEE Trans. Antennas Propag.* **2020**, *68*, 6003–6012. [CrossRef]
31. Khorasaninejad, M.; Chen, W.T.; Devlin, R.C.; Oh, J.; Zhu, A.Y.; Capasso, F. Metalenses at visible wavelengths: Diffraction-limited focusing and subwavelength resolution imaging. *Science* **2016**, *352*, 1190–1194. [CrossRef]
32. Chen, B.H.; Wu, P.C.; Su, V.C.; Lai, Y.C.; Chu, C.H.; Lee, I.C.; Chen, J.W.; Chen, Y.H.; Lan, Y.C.; Kuan, C.H.; et al. GaN metalens for pixel-level full-color routing at visible light. *Nano Lett.* **2017**, *17*, 6345–6352. [CrossRef] [PubMed]
33. Zhang, W.; He, H.; Li, H.; Duan, L.; Zu, L.; Zhai, Y.; Li, W.; Wang, L.; Fu, H.; Zhao, D. Visible-light responsive TiO_2-based materials for efficient solar energy utilization. *Adv. Energy Mater.* **2021**, *11*, 2003303. [CrossRef]
34. Li, Y.; Fan, X.; Huang, Y.; Guo, X.; Zhou, L.; Li, P.; Zhao, J. Dielectric Metalens for Superoscillatory Focusing Based on High-Order Angular Bessel Function. *Nanomaterials* **2022**, *12*, 3485. [CrossRef] [PubMed]
35. Zhao, M.; Yu, B.; Du, J.; Wen, J. Focusing Characteristics and Widefield Imaging Performance of the Silicon Metalens in the Visible Range. *Micromachines* **2022**, *13*, 1183. [CrossRef]
36. Alnakhli, Z.; Lin, R.; Liao, C.H.; El Labban, A.; Li, X. Reflective metalens with an enhanced off-axis focusing performance. *Opt. Express* **2022**, *30*, 34117–34128. [CrossRef] [PubMed]
37. Bao, Q.; Loh, K.P. Graphene photonics, plasmonics, and broadband optoelectronic devices. *ACS Nano* **2012**, *6*, 3677–3694. [CrossRef]
38. Lin, H.; Xu, Z.Q.; Cao, G.; Zhang, Y.; Zhou, J.; Wang, Z.; Wan, Z.; Liu, Z.; Loh, K.P.; Qiu, C.W.; et al. Diffraction-limited imaging with monolayer 2D material-based ultrathin flat lenses. *Light. Sci. Appl.* **2020**, *9*, 137. [CrossRef]
39. Zheng, X.; Jia, B.; Lin, H.; Qiu, L.; Li, D.; Gu, M. Highly efficient and ultra-broadband graphene oxide ultrathin lenses with three-dimensional subwavelength focusing. *Nat. Commun.* **2015**, *6*, 8433. [CrossRef]
40. Kong, X.T.; Khan, A.A.; Kidambi, P.R.; Deng, S.; Yetisen, A.K.; Dlubak, B.; Hiralal, P.; Montelongo, Y.; Bowen, J.; Xavier, S.; et al. Graphene-based ultrathin flat lenses. *ACS Photonics* **2015**, *2*, 200–207. [CrossRef]
41. Yang, J.; Wang, Z.; Wang, F.; Xu, R.; Tao, J.; Zhang, S.; Qin, Q.; Luther-Davies, B.; Jagadish, C.; Yu, Z.; et al. Atomically thin optical lenses and gratings. *Light. Sci. Appl.* **2016**, *5*, e16046. [CrossRef]
42. Guo, H.; Yue, S.; Wang, R.; Hou, Y.; Li, M.; Zhang, K.; Zhang, Z. Design of polarization-independent reflective metalens in the ultraviolet–visible wavelength region. *Nanomaterials* **2021**, *11*, 1243. [CrossRef]
43. Wu, L.; Tao, J.; Zheng, G. Controlling phase of arbitrary polarizations using both the geometric phase and the propagation phase. *Phys. Rev. B* **2018**, *97*, 245426. [CrossRef]
44. Yang, H.; Li, G.; Su, X.; Cao, G.; Zhao, Z.; Chen, X.; Lu, W. Reflective metalens with sub-diffraction-limited and multifunctional focusing. *Sci. Rep.* **2017**, *7*, 12632. [CrossRef]

45. Guo, Z.; Zhu, L.; Shen, F.; Zhou, H.; Gao, R. Dielectric metasurface based high-efficiency polarization splitters. *RSC Adv.* **2017**, *7*, 9872–9879. [CrossRef]
46. Zuo, H.; Choi, D.Y.; Gai, X.; Ma, P.; Xu, L.; Neshev, D.N.; Zhang, B.; Luther-Davies, B. High-efficiency all-dielectric metalenses for mid-infrared imaging. *Adv. Opt. Mater.* **2017**, *5*, 1700585. [CrossRef]
47. Mahmood, N.; Kim, I.; Mehmood, M.Q.; Jeong, H.; Akbar, A.; Lee, D.; Saleem, M.; Zubair, M.; Anwar, M.S.; Tahir, F.A.; et al. Polarisation insensitive multifunctional metasurfaces based on all-dielectric nanowaveguides. *Nanoscale* **2018**, *10*, 18323–18330. [CrossRef]
48. Park, C.S.; Shrestha, V.R.; Yue, W.; Gao, S.; Lee, S.S.; Kim, E.S.; Choi, D.Y. Structural color filters enabled by a dielectric metasurface incorporating hydrogenated amorphous silicon nanodisks. *Sci. Rep.* **2017**, *7*, 2556. [CrossRef]
49. Khorasaninejad, M.; Shi, Z.; Zhu, A.Y.; Chen, W.T.; Sanjeev, V.; Zaidi, A.; Capasso, F. Achromatic metalens over 60 nm bandwidth in the visible and metalens with reverse chromatic dispersion. *Nano Lett.* **2017**, *17*, 1819–1824. [CrossRef] [PubMed]
50. Yang, Y.; Yoon, G.; Park, S.; Namgung, S.D.; Badloe, T.; Nam, K.T.; Rho, J. Revealing structural disorder in hydrogenated amorphous silicon for a low-loss photonic platform at visible frequencies. *Adv. Mater.* **2021**, *33*, 2005893. [CrossRef] [PubMed]
51. Yoon, G.; Lee, D.; Nam, K.T.; Rho, J. "Crypto-display" in dual-mode metasurfaces by simultaneous control of phase and spectral responses. *ACS Nano* **2018**, *12*, 6421–6428. [CrossRef]
52. Fischer, B.; Beyer, W.; Lambertz, A.; Nuys, M.; Duan, W.; Ding, K.; Rau, U. The microstructure of underdense hydrogenated amorphous silicon and its application to silicon heterojunction solar cells. *Sol. RRL* **2023**, *7*, 2300103. [CrossRef]